Design and evaluation of short armature core double-sided transverse flux type PMLSM

Jung-Seob Shin*, Takafumi Koseki*, and Houng-Joong Kim**
*The University of Tokyo, Engineering Building #2 12F, 7-3-1 Hongo, Bunkyo-ku, Tokyo 113-8656, Japan
**KOVERY Co. Ltd, 987-4, Gosaek-dong, Gwonseon-gu, Suwon, Gyeonggi-do, 441-813, Korea

***Abstract*-- In this paper, design and evaluation of short armature core double-sided transverse flux type PMLSM. First, structure and operational principle of the proposed model are introduced. Theoretical design for calculating thrust is then proposed for a design of core-pole combination, skewing, and chamfering. Finally, thrust is numerically evaluated through field calculations using 3-D finite element method.**

***Index Terms*-- Analytical design, Field calculation, permanent magnet linear synchronous motor, transverse flux machinery.**

I. Introduction

Direct linear drives have been of great interest in industries, compared with mechanical rotary-translational conversion of motion such as ball-skrew drive.

Especially, the permanent magnet linear synchronous motor (PMLSM) has contributed to the popularization in industrial fields due to the advent of rare earth permanent magnet.

Large thrust density is an important technical performance requirement for PMLSMs. The transverse flux type machinery (TFM) is can be a good solution [1]-[2]. However, conventional TFMs have a relatively complex structure that requires relatively large manufacturing effort [3].

The authors have proposed double-sided transverse flux type PMLSM as a simple transverse flux solution for easy manufacturing [4].

In this paper, design and evaluation of the proposed model is conducted. In the design and evaluation, thrust considering core-pole combination is both theoretically and numerically analyzed by magnetic circuit method and field calculation using the 3-D finite element method (FEM), respectively. Also, simple estimation of thrust considering skewing and chamfering of the field magnet is conducted. Finally, an effect of skewing and chamfering on thrust and detent force is verified. In the field calculation, the JMAG-Designer 10.4.3h, a well-known commercial package, has been used [5].

II. Basic Structure and Operational Principles

Fig. 1 shows the fundamental configuration of a three-phase unit of the proposed short armature core double-sided transverse flux type PMLSM. An armature unit can be assembled by inserting two square-shaped iron cores into a non-magnetic material box, as shown in Fig. 1(a). A field unit consists of four magnets, a square-shape iron core as back-iron on both sides, as shown in Fig. 1 (b).

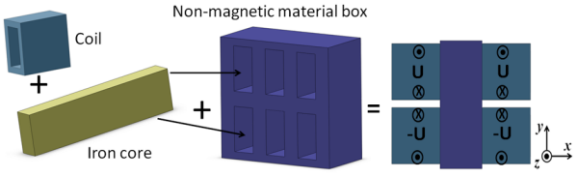

(a) An armature unit (mover)

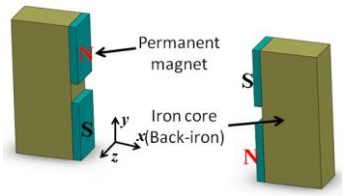

(b) A field unit (stator)

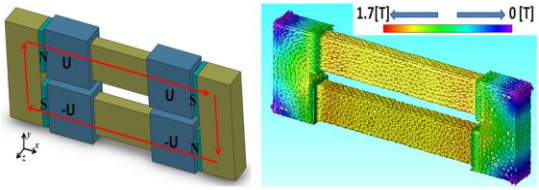

(c) A magnetic circuit (In (c), the red arrows denote flux flow; the non-magnetic material box was removed for easy understanding.)

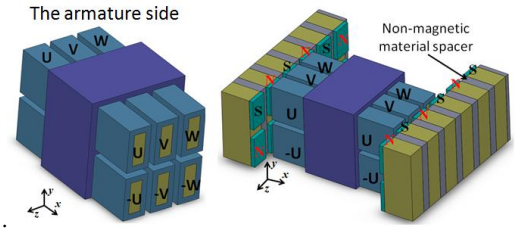

(d) Configuration along the moving direction

Fig. 1. Fundamental configuration of the three-phase unit.

Inserting an armature core into the non-magnetic material box creates two armature tooth on both sides. The armature coils are then inserted into each armature teeth.

A magnetic circuit comprises an inserted armature unit and a field unit, as shown in Fig. 1 (c). Flux from the north pole flows into the south pole along the short armature core. Two coils in the lower side are wound in a direction opposite to the two coils in the upper side, and

these coils are connected in series. By applying current to these coils, they are excited with 180-phase difference.

The armature cores are arranged along the moving direction *z*, as shown in Fig. 1 (d). Each armature core is spatially separated by 120 degrees difference. The field magnets are arranged along the moving direction *z* with a non-magnetic spacer, and each magnet is electrically separated by 180 degrees. The non-magnetic material spacer isolates the magnetic paths.

The proposed model operates as a three-phase AC synchronous motor by applying AC current which has 120-degree phase differences to each armature coil. Here, -U, -V, and -W are the current components shifted 180 degrees from U, V, and W [4].

III. Design of Thrust for Simple Estimation

In a theoretical design for a simple estimation, the authors have focused on the thrust behavior in a one-core based configuration. This is because the thrust behavior in a three-phase configuration can be estimated by superposing the results of the one-phase configuration.

The authors have employed a magnetic circuit method and made the following assumptions for a simplified theoretical evaluation of thrust [6]-[7].

(a) The air gap flux density B_g is the same as the magnet flux density B_m and its distribution is constant regardless of the slot effect.
(b) In the calculation of B_m, the air gap length l_{gc} applied Carter's factor is used to compensate for the slot effect.
(c) Permeability of the iron cores is infinitely large. Magnetic saturation is negligible.

A. Variables Employed in the Design

Variables employed in the design are shown in Fig. 2 and Table I.

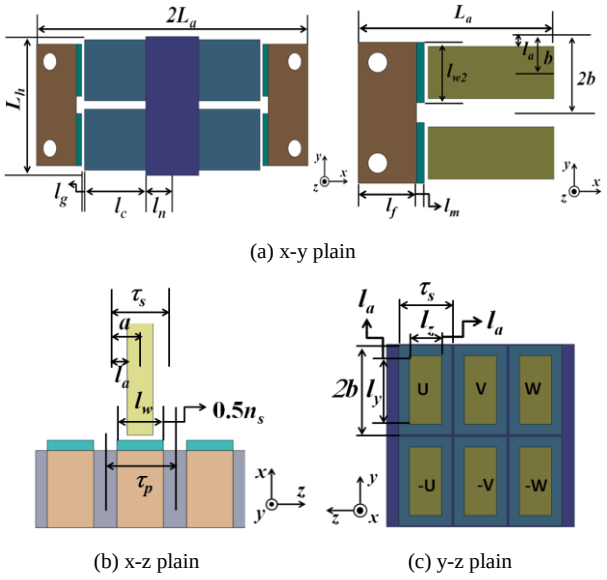

(a) x-y plain

(b) x-z plain

(c) y-z plain

Fig. 2. Variables employed in the design (In (a) and (b), the armature coils are removed for clarity. Also, variables are labeled in the half side because of symmetric structure.).

The authors have focused on l_a and l_m defined in Fig. 2(a). Thrust is generally expressed as the product of the electric loading and magnetic loading. When dimensions in other parts are kept constant, l_a and l_m affect the electric and magnetic load, respectively. The larger l_a is, the larger the winding turn number per an armature pole can be achieved in the designated slot pitch. It represents the increase of the electrical load by increasing the magnetomotive force (MMF). On the other hand, the larger l_m is, the larger the flux density in magnet at operating point can be achieved in the designated volume. But, the winding turn number per armature pole is decreased. For that reason, it is important to estimate the point where the product of the electric loading and magnetic loading is maximum value in the designated volume.

TABLE I
Variables Employed in the Design

Symbol	Note
L_a	Half-length in cross-section
L_h	Height in cross-section
τ_p	Pole pitch
τ_s	Slot pitch
l_w	Magnet length to z-direction
l_{w2}	Magnet length to y-direction
l_f	Back yoke length to x-direction
l_n	Half-length of non-magnetic material box
n_s	Length of non-magnetic spacer
a	Half-length of core pitch
b	Length of a quarter of the height
l_c	Half-length of core pitch
l_g	Mechanical air gap length
l_a	Half-length of slot
l_m	Magnet length in the magnetization direction

B. Flux Flowing to the Armature Core

The magnetic circuit equation for the magnetic path illustrated in Fig. 1(c) is written as (1) from the assumptions. In (1), H_m and H_g are the magnetic-field component of the magnet and the air gap, respectively, R_g is the magnetic reluctance in the air gap and ϕ_g is the air gap flux.

$$H_m l_m + H_g l_{gc} = H_m l_m + R_g \phi_g = 0 \tag{1}$$

From (1), H_m can be expressed as (2). In (2), μ_0 is the permeability of air.

$$H_m = -\frac{B_m l_{gc}}{\mu_0 l_m} \tag{2}$$

Here, B_m at operating point is (3). B_r is remanence of the field magnet. By substituting (2) into (3), B_m under a no-load condition can be expressed as (4).

$$B_m = B_r + \mu_0 H_m \tag{3}$$

$$B_m = B_g = B_r \Big/ \left(1 + \frac{l_{gc}}{l_m}\right) \tag{4}$$

The flux flowing from the field magnet to the armature core ϕ_a is calculated as (5). $A_a(l_a)$ is the cross-section of an armature core.

$$\phi_a(l_a) = B_g \times A_a(l_a)$$
$$(\ \because A_a(l_a) = 4(a - l_a) \times (b - l_a)\ ) \tag{5}$$

If all the $\phi_a(l_a)$ is linking to an armature coil and B_g by moving an armature unit is simplified as shown in Fig. 3, the total amount of effective flux linking to an armature coil ψ_c can be expressed as Fourier series. Its maximum value considered the fundamental component is (6). In (6), $N(l_a, l_c)$ is the number of winding turns per an armature teeth, $A_w(l_a, l_c)$ is the dimension of the cross-section in which the armature coil is wound, $\alpha(l_a, l_c)$ and S_c are the lamination factor of the coil and the dimension of a conductor, respectively. Also, $k_c(l_a)$ is coefficient that indicates the ratio of total magnetic flux linking to an armature coil.

From (6), it is found that ψ_c is gradually decreased after a certain point with the increase of l_a. This means that flux from the north pole will be leaked to the south pole next to the north pole although the number of winding turns per an armature teeth is increased with the increase of l_a.

$$\Psi_c(l_a) = N(l_a, l_c)\phi_a(l_a) = \frac{4N(l_a, l_c)k_c(l_a)B_g A_a(l_a)}{\pi} \sin\left(\frac{\pi(a - l_a)}{\tau_p}\right)$$
$$\left(\therefore N(l_a, l_c) = \frac{\alpha(l_a, l_c)A_w(l_a, l_c)}{S_c}, k_c(l_a) = \frac{A_a(0) - A_a(l_a)}{A_a(l_a)}\right) \tag{6}$$

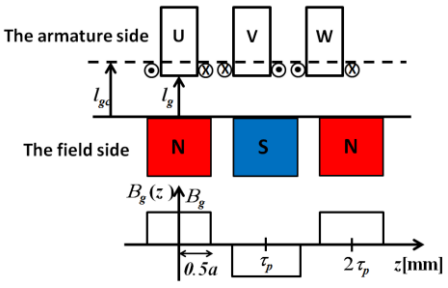

Fig. 3. Flux density distribution resulting from moving an armature unit.

C. Maximum Thrust

In the control under the condition that *d*-axis current is maintained to zero, maximum thrust per an armature unit can be expressed as (7). It means that maximum thrust generates in the position where electrical phase difference between the armature core and the north pole is 90 degrees. In (7), E_{rms} is the RMS value of the back EMF, p is the number of poles in a field unit, I is armature current, and v and J are moving velocity and current density, respectively.

From (7), when other variables are fixed, the optimal design for thrust means finding the point where multiplication of electric load and magnetic load reaches maximum value in the designated volume.

$$F_t(l_a) = p\frac{E_{rms}I}{v} = \frac{2\sqrt{2}pk_c(l_a)B_m A_a(0)N(l_a, l_c)I}{\tau_p} \sin\left(\frac{\pi(a - l_a)}{\tau_p}\right)$$
$$\left(\therefore N(l_a, l_c)I = \frac{\alpha(l_a, l_c)A_w(l_a, l_c)I}{S_c} = \alpha(l_a, l_c)A_w(l_a, l_c)J\right) \tag{7}$$

D. Maximum Thrust per Three-phase Considering Core-pole Combination

In the design of core-type PMLSM, detent force reduction is one of the important aspects because large detent force causes thrust ripple, which results in a poor positioning accuracy.

Detent force can be significantly reduced by the proper selection of core-pole combination [8]. Maximum thrust considering core-pole combination can be expressed as (8). In (8), 1.5 means the total amount of thrust in the case of general three phase machine, m is the number of armature unit per a phase, and α is a coefficient that is the ratio of thrust based on thrust in the general three core-two pole combination.

$$F_{t\_3phase}(l_a) = 1.5 \times m \times \alpha \times F_t(l_a) \tag{8}$$

The authors have experienced that detent force in nine core-eight pole combination can be significantly reduced up to about 35 % of that in nine core-six pole combination based on the general three core-two pole combination [9]. For that reason, the authors have applied nine core-eight pole combination to the proposed model.

When comparing with nine core-six pole combination based on three core-two pole combination, α is 0.922. This means maximum thrust per three-phase in nine core-eight pole combination is about 8% smaller than that nine core-six pole combination. This is result from asymmetric characteristic in nine core-eight pole combination that thrust per each core in a phase has electrical phase differences of 20 degrees, as shown Fig. 4. For that reason, maximum thrust per three cores in a phase is generated in the position where electrical phase difference between the armature core and the north pole is 70 electrical degrees.

The proposed nine core-eight pole combination has advantage even when the trade-off between large thrust and detent force reduction is considered in the design of core-type PMLSM. The authors have chose 100 × 40 × 108 mm^3 as the total volume in nine core-eight pole combination. The consequent design parameters in the proposed model are shown in Table II.

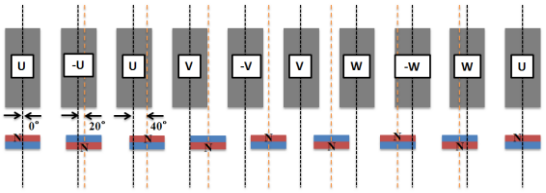

(a) Nine core-eight pole combination

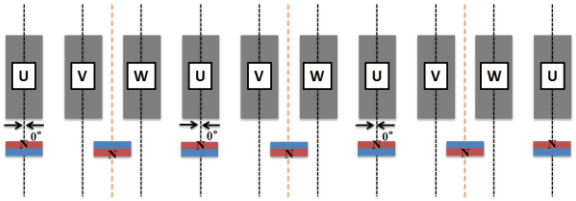

(b) Nine core-six pole combination

Fig. 4. Two types of core-pole combination.

TABLE II
DESIGN PARAMETERS IN THE PROPOSED MODEL

Symbol	Quantity	Symbol	Quantity
L_a	50 [mm]	n_s	4.5 [mm]
L_h	40 [mm]	a	6 [mm]
τ_p	13.5 [mm]	b	10 [mm]
τ_s	12 [mm]	l_c	Variable
l_w	9 [mm]	l_g	1 [mm]
l_{w2}	15 [mm]	l_a	Variable
l_f	15 [mm]	l_m	Variable
l_n	10 [mm]	v	1 [m/s]
J	7 [A/mm^2]	I	3.4 [A]
S_c	0.804 × 0.804 [mm] (conductor: 0.7 × 0.7)	B_r	1.32 [T]

IV. NUMERICAL ANALYSIS OF THRUST

The authors have applied 3-D FEM field calculation to the proposed model in order to analyse thrust numerically. The 3-D mesh model is shown in Fig. 5. In the calculation of thrust, an armature unit was selected and periodic boundary condition was applied to save computation time.

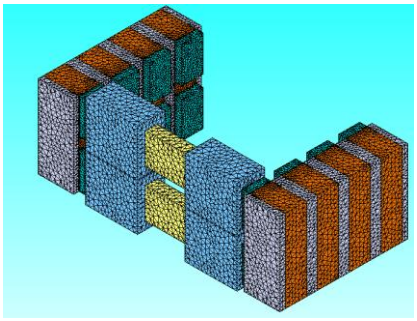

Fig. 5. The three-dimensional mesh model in the FEM calculation.

The result is shown in Fig. 6. Thrust decreases from l_a=3.5 mm because of the decreasing flux linkage to the armature coil, regardless of spatially increased MMF. The authors have decided on l_a=3.5 mm as the point at which large thrust can be obtained.

However, detent force was larger than thrust from l_m=4 mm, as shown in Fig. 6 (b) and (c). This means the magnetic load affected by the field magnet was larger than the electrical load affected by the MMF.

From the results in Fig. 6, the ratio of detent force was improved with the decrease of l_m and has a value of less than one at l_m=2 mm. When considering a design for high thrust and low detent force within a designated volume, a good point was at l_m=2 mm and l_a=3.5 mm. In this point, the number of winding turns per an armature teeth is 112 turns.

Table III shows thrust and detent force in nine core-eight pole combination. The maximum thrust per three-phase is 116.7 N. Although detent force per a armature core is large, it is significantly reduced to 3.2 % of thrust by applying nine core-eight pole combination.

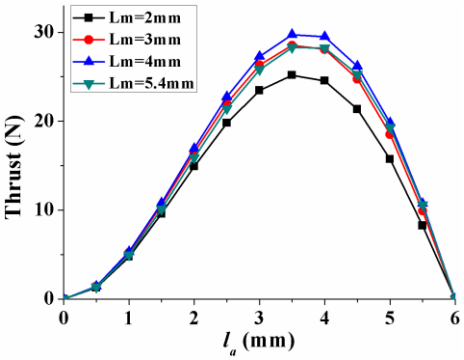

(a) Theoretical result of thrust

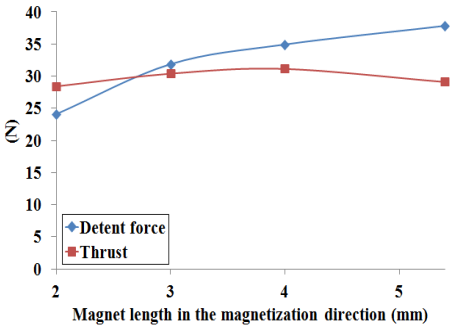

(b) Thrust and detent force based on 3-D FEM result at l_a=3.5mm

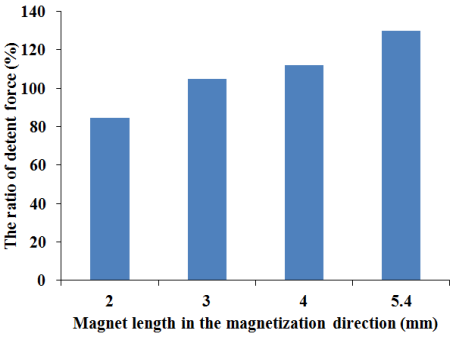

(c) Ratio of detent force to thrust based on 3-D FEM result at l_a=3.5mm

Fig. 6. The theoretical and FEM results of thrust and detent force.

TABLE III
THRUST AND DETENT FORCE IN NINE CORE-EIGHT POLE COMBINATION

Thrust [N]	Detent [N]	Ratio of detent force to thrust [%]
116.7	3.7	3.2

V. ANALYSIS OF THRUST AND DETENT FORCE BY SKEWING AND CHAMFERING

Detent force can be also decreased with skewing and chamfering of the field magnet because they mitigate a

change of magnetic co-energy in the air gap between the field magnets and armature tooth [10].

However, the disadvantages of skewing and chamfering are that they could reduce thrust and increase manufacturing complexity [11]. For that reason, it is important to verify the effect of skewing and chamfering on thrust and detent force in the initial design stage.

The authors have applied skewing and chamfering to nine core-eight pole combination. In this section, a simple estimation of thrust considering skewing and chamfering of the field magnet is conducted. Also, the effectiveness of skewing and chamfering on thrust and detent force is evaluated by ratio of detent force to thrust. Detent force has been calculated from 3-D FEM field analysis.

A. *Estimation of Thrust*

Fig. 7 shows skewing and chamfering applied to the field magnet. In Fig. 7, θ_{sk} and θ_{cf} denote skewing and chamfering angle, respectively. Also, θ_{cf} can be expressed as the distance l_s.

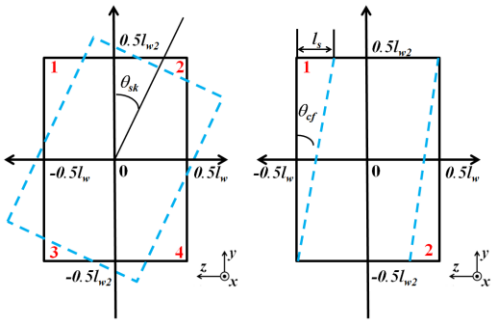

(a) Skewing (b) Chamfering

Fig. 7. Skewing and chamfering. (The dashed lines denote skewed and chamfered magnets.)

In (7), it is found that thrust is proportional to the effective flux linking to the armature coil. The authors have considered that the decrease ratio of the effective flux in skewing and chamfering can be simply estimated by subtracting the flux in the dimension where skewed or chamfered magnet is not faced with their original position from the flux in their original position.

They can be calculated from the sum of dimension in each part, as expressed in (9) and (10). In (9) and (10), S_i is the area where skewed or chamfered magnet is not faced with their original position, as labeled in red numbers in Fig. 7. Also, subscript *sk* and *cf* mean skewing and chamfering, respectively.

$$S_{sk}(\theta_{sk}) = \sum_{i=1}^{4} S_i$$

$$= \tan\frac{\theta_{sk}}{2}\left[\left(\frac{\tau_p - n_s}{2} - \frac{l_{w2}}{2}\tan\frac{\theta_{sk}}{2}\right)^2 + \left(\frac{l_{w2}}{2} - \frac{\tau_p - n_s}{2}\tan\frac{\theta_{sk}}{2}\right)^2\right] \quad (9)$$

$$S_{cf}(\theta_{cf}) = \sum_{i=1}^{2} S_i = l_{w2}^2 \tan\theta_{cf} \quad (10)$$

From (9) and (10), the decrease ratio of the effective flux can be expressed as (11). The authors have defined (11) as the skewing and chamfering coefficient. Thrust considering skewing and chamfering can be simply estimated from multiplying (7) by (11).

$$C_{sk}(\theta_{sk}) = \frac{S_{sk}(0) - S_{sk}(\theta_{sk})}{S_{sk}(0)}, \quad C_{cf}(\theta_{cf}) = \frac{S_{cf}(0) - S_{cf}(\theta_{cf})}{S_{cf}(0)} \quad (11)$$

B. *Analysis of Thrust and Detent Force by Skewing and Chamfering*

Fig. 8 and 9 show the results of thrust and detent force in nine core-eight pole combination when skewing and chamfering are applied. Also, Table IV shows the value of l_s and θ_{cf} employed in analysis.

In Fig. 8, thrust decreases with an increase of θ_{sk} and l_s and the error between theoretical values and FEM values is small. Especially, the decrease of thrust in chamfering is larger than that in skewing. This is because the decrease of the flux from the field magnet by chamfering is larger than that by skewing, which causes a decrease of effective flux and finally results in a decrease of thrust.

TABLE IV
CHAMFERING ANGLE θ_{cf} AND L_S

l_s [mm]	θ_{cf} [deg]
0	0
1.5	5.7
2.5	9.5
3.5	13.1

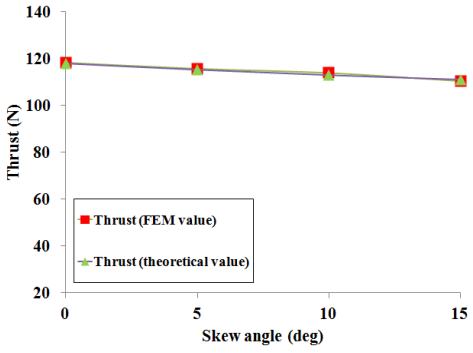

(a) Skewing

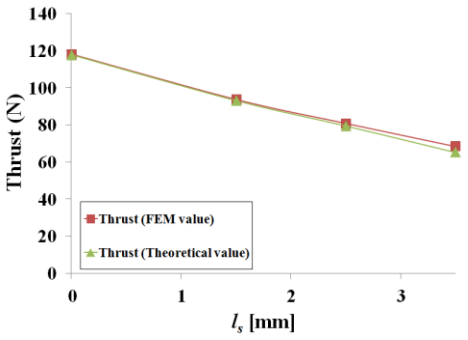

(b) Chamfering

Fig. 8. The theoretical and FEM results in skewing and chamfering.

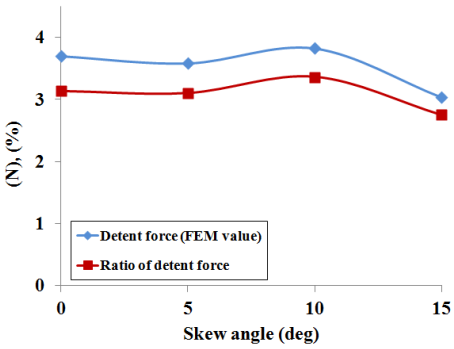

(a) Skewing

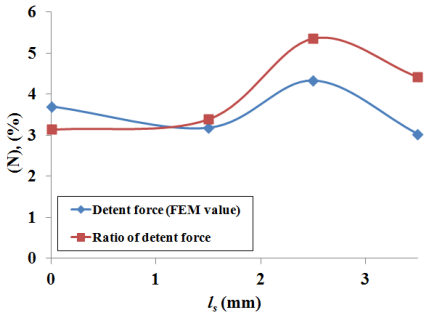

(b) Chamfering

Fig. 9. Ratio of detent force to thrust based on 3-D FEM results.

Detent force decreases with an increase of θ_{sk} and l_s, except near 10 degrees, as shown in Fig. 9. As in the case of thrust, the decrease ratio of detent force in chamfering is larger than that in skewing because of small magnetic co-energy stored in the air gap.

However, the ratio of detent force to thrust increases in chamfering. This means that a decrease of thrust is more significant than a decrease of detent force and large thrust ripple would be eventually generated. Although there is an improvement in skewing, it is not large value when considering manufacturing complexity. For that reason, the authors have decided not to apply skewing and chamfering to the proposed model.

VI. Conclusion

In this paper, design and evaluation of the proposed short armature core double-sided transverse flux type PMLSM has been conducted. Thrust considering core-pole combination has been both theoretically and numerically analyzed using magnetic circuit method and field calculation using the 3-D FEM, respectively.

Thrust is proportional to the multiplication of armature magnetomotive force and the field magnet flux density. Based on this fact, this paper has proposed a design method to find the optimal point where maximum thrust can be obtained in a limited space for the proposed motor. The optimal design for thrust means finding the point where multiplication of electric load and magnetic load reaches maximum value. The maximum thrust per three-phase is 116.7 N. Although detent force per a armature core is large, it is significantly reduced to 3.2 % of thrust by applying nine core-eight pole combination.

Also, the effect of skewing and chamfering of the field magnet on thrust and detent force has been verified in nine core-eight pole combination. A simple estimation of thrust considering skewing and chamfering has been conducted. Theoretical values agree rather well with FEM values.

In the proposed model, detent force decreases with the increase of skewing and chamfering angle because they mitigate a change of magnetic co-energy in the air gap. Also, thrust decreases with skewing and chamfering due to a decrease of the effective flux.

However, there was no significant effect of applying skewing and chamfering when considering manufacturing complexity and the trade-off between large thrust and detent force reduction. Therefore, the authors decided not to apply skewing and chamfering in nine core-eight pole combination to the proposed model.

References

[1] H. Weh, H. Hoffman, and J. Landrath, “New permanent magnet excited synchronous machine with high efficiency at low speeds,” in Proc. *Int. Conf. Elect. Mach.*, 1988, pp. 35-40.

[2] J.H. Chang, D.H. Kang, J.Y. Lee, and J.P. Hong, “Development of transverse flux linear motor with permanent magnet excitation for direct drive applications,” *IEEE Trans. Magn.*, vol. 41, no. 5, pp. 1936–1939, May 2005.

[3] S. D. Joao and V. Mauricio, “Transverse flux machine : what for? ”, *IEEE Multidisciplinary Engineering Education Magazine*, Vol. 2,No. 1, pp. 4-6, March 2007.

[4] J. S. Shin, T. Koseki, and H. J. Kim, “Proposal and design of short armature core double-sided transverse flux type linear synchronous motor”, *IEEE Trans. Magn.*, 2012 (To be published).

[5] JSOL Corp. http://www.jmag-international.com/.

[6] Krishnan Ramu, *Permanent Magnet Synchronous and Brushless DC Motors*, CRC Press/Taylor & Francis, 2009.

[7] Jacek F. Gieras and Zbigniew J. Piech, *Linear synchronous motors: transportation and automation systems*, CRC Press, 1999.

[8] J. Jung, J. Hong, and Y. Kim, “Characteristic Analysis and Comparison of IPMSM for HEV According to Pole and Slot Combination”, *IEEE Vehicle Power and Propulsion Conference*, VPPC 2007, pp. 778-783, 2007.

[9] T. Nakamura, J. S. Shin, and T. Koseki, “Cogging force reduced by pole-slot combinations in a transverse-flux type Permanent Magnet Linears Synchronous Motor”, *IEEJ Linear Drive Technical Meeting*, LD-11-030, 2011. (written in Japanese)

[10] Z. Guo, L. Chang, Y. Xue, “Cogging torque of permanent magnet electric machines: an overview”, Canadian Conference Electrical and Computer Engineering, CCECE '09, pp. 1172-1177, 2009.

[11] Hwang I. C, Jang K. B, and Kim G. T, “A study on the characteristics analysis according to overhang and skew of permanent magnet in PMLSM”, *Proceeding of International Conference on Electrical Machines*, ICEMS 2007, pp. 1255-1258, 2007.